Research Square

Preprints are preliminary reports that have not undergone peer review.
They should not be considered conclusive, used to inform clinical practice,
or referenced by the media as validated information.

The Dynamics of a Four-Step Feedback Procedure to Control Chaos

Jose S. Cánovas (jose.canovas@upct.es)
Universidad Politecnica de Cartagena https://orcid.org/0000-0002-2854-5833

Research Article

Keywords: Chaos, topological entropy, Parrondo's paradox

Posted Date: March 15th, 2021

DOI: https://doi.org/10.21203/rs.3.rs-295959/v1

License: This work is licensed under a Creative Commons Attribution 4.0 International License.
Read Full License

The dynamics of a four-step feedback procedure to control chaos

Jose S. Cánovas*

March 3, 2021

Abstract

In this paper we make a description of the dynamics of a four-step procedure to control the dynamics of the logistic map. Some massive calculations are made for computing the topological entropy with prescribed accuracy. This provides us the parameter regions where the model has a complicated dynamical behavior. Our computations also show the dynamic Parrondo's paradox "simple+simple=complex", which should be taking into account to avoid undesirable dynamics.

1 Introduction

In [18], a four-step feedback procedure to control a chaotic map proposed by [24] is studied. In particular, the authors consider the logistic map $f_\mu(x) = \mu x(1-x)$ and the scheme

$$\begin{cases} x_{n+1} = (1-\lambda_3)y_n + \lambda_3 f_\mu(y_n) = g_{\lambda_3,\mu}(y_n), \\ y_n = (1-\lambda_2)z_n + \lambda_2 f_\mu(z_n) = g_{\lambda_2,\mu}(z_n), \\ z_n = (1-\lambda_1)x_n + \lambda_1 f_\mu(x_n) = g_{\lambda_1,\mu}(x_n), \end{cases}$$

which can be rewritten as

$$x_{n+1} = F_{\lambda_1,\lambda_2,\lambda_3,\mu}(x) = (g_{\lambda_3,\mu} \circ g_{\lambda_2,\mu} \circ g_{\lambda_1,\mu})(x_n). \tag{1}$$

They analyze a switching strategy to control chaos which can lead to the Parrondo's paradox "chaos1 + chaos2 = order" or "undesirable1 + undesirable2= desirable" dynamical behavior. Roughly speaking (see e.g. [7]), we consider two discrete

*Department of Applied Mathematics and Statistics, Technical University of Cartagena, C/ Doctor Flemming sn, 30.202, Cartagena, Spain. Email: Jose.Canovas@upct.es

dynamical systems given by continuous maps $f_i : X \to X$, $i = 1, 2$, on a metric space X, usually a subset of $\mathbb{R}^n$, $n \in \mathbb{N}$. The Parrondo's paradox appears when the dynamical behavior of both maps is simple (resp. chaotic) and that of $f_1 \circ f_2$ is chaotic (resp. simple). Of course, this paradox can involve more maps (see e.g. [5]). Mathematical examples includes interval dynamics (see [8] and [5]), dynamics of complex maps (see [2] and [3]), local stability problems ([14] and [16]) among others. In addition, we can find applications of this paradox to Physics (see [12] and [19]), Biology (see [23], [25] and [26]) and Social Sciences (see [13] and [20]).

It is stated in [18] that "the range of stability of the dynamical system can be increased by using the switching strategy". This is shown by simulations where μ takes two different values, but identical values of λ_i, $i = 1, 2, 3$. We think that the control parameter should vary instead of μ, because the system that we want to control depends on this parameter.

However, for a fixed value of μ they analyze just the case $\lambda_1 = \lambda_2 = \lambda_3 = \lambda$. In this case, the model (1) reads as

$$x_{n+1} = F_{\lambda,\lambda,\lambda,\mu}(x) = g^3_{\lambda,\mu}(x_n). \tag{2}$$

Hence, no paradox is possible here and the dynamics it given by the third iterate $g^3_{\lambda,\mu}$, which has a similar behavior to that of the map $g_{\lambda,\mu}$. Probably, they made the assumption on λ because the proposed model depends on four parameters and then, as we will show, two problems appear in order to study the model. On one hand, four parameters implies that the computations increase. For instance, if we fix $\lambda_i \in (0, 1)$, $i = 1, 2, 3$, and $\mu \in [3, 4]$ with step size 0.01, the number of cases under study is 10^8, while for $\lambda_1 = \lambda_2 = \lambda_3 = \lambda$ is just the middle. On the other hand, presenting the results is quite complicated because usually bifurcation diagrams are showed in dimension two and graphs of functions, e.g. the estimation of Lyapunov exponents, only can be done in dimension three.

The aim of this paper is to analyze properly the system, including the general cases. We will make use of the topological entropy, which allows us to compute the parameter regions where the dynamics is complicated with prescribed accuracy. As a necessary complement, we will also estimate the Lyapunov exponents. We cannot make anything to reduce the number of parameters, so we will fix some of them, changing the remaining ones in order to see the evolution of chaotic parametric regions. For that, we previously make an study of the map $F_{\lambda_1,\lambda_2,\lambda_3,\mu}$, because its shape has influence in the techniques we have to use to make our analysis.

The paper is organized as follows. Next section will be devoted to study the map $F_{\lambda_1,\lambda_2,\lambda_3,\mu}$ and establish some basic facts which we use to analyze the model. This will be done in Section 3, where we distinguish two particular cases, namely $\lambda_1 = \lambda_2 = \lambda_3$ and $\lambda_1 = \lambda_2$, and the general one. The paper finishes with some conclusions.

2 Model facts

Let $f_\mu(x) = \mu x(1-x)$ be he logistic family where $\mu > 0$ and x a real number. It is well-known that if $\mu \leq 4$, then the interval $I = [0,1]$ is invariant by f_μ, that is, $f_\mu(I) \subseteq I$. It is easy to see that for any $x \in \mathbb{R} \setminus [0,1]$ its orbit converges to $-\infty$. If $\mu > 4$, the interval I is not invariant because there exists a (maximal) interval $I_0 = (a,b)$, containing $1/2$, such that $f_\mu(I_0) \subset (-\infty, 0)$, and so any orbit with initial condition in I_0 converges to $-\infty$ as well. In fact, in this case almost every orbit in I converges to $-\infty$, although the map f_μ is chaotic since $\{[0,a],[b,1]\}$ is a two-horseshoe and therefore f_μ has positive topological entropy (see [1, Chapter 4]). The chaotic set, that is, the set where f_μ has a complicated dynamical behavior lies in a zero measure subset of I. Then, we will restrict our analisys to the case $\mu \in (0,4]$.

So, fix $g_{\lambda,\mu}(x) = (1-\lambda)x + \lambda f_\mu(x)$, $\lambda \in [0,1]$. Note that $g_{\lambda,\mu}$ leaves invariant the interval I because it is a convex combination of two points x and $f_\mu(x)$ lying in this interval. However, for practical reasons we may consider the map restricted to the interval $[0,c]$, where c is the smallest positive real number such that $g_{\lambda,\mu}(c) = 0$. Now, we consider the map under study

$$F_{\lambda_1,\lambda_2,\lambda_3,\mu} = g_{\lambda_3,\mu} \circ g_{\lambda_2,\mu} \circ g_{\lambda_1,\mu}.$$

This map also leaves invariant the interval I, but again for practical reasons, we consider it as defined in $[0,c]$, where where c is the smallest positive real number such that $F_{\lambda_1,\lambda_2,\lambda_3,\mu}(c) = 0$. This will simplify somehow the description below.

We need to compute the local extrema of $F_{\lambda_1,\lambda_2,\lambda_3,\mu}$, given by the equation

$$F'_{\lambda_1,\lambda_2,\lambda_3,\mu}(x) = 0,$$

which reads as

$$g'_{\lambda_3,\mu}((g_{\lambda_2,\mu} \circ g_{\lambda_1,\mu})(x)) \cdot g'_{\lambda_2,\mu}(g_{\lambda_1,\mu}(x)) \cdot g'_{\lambda_1,\mu}(x) = 0,$$

which gives us the equations

$$g'_{\lambda_1,\mu}(x) = 0, \tag{3}$$

$$g'_{\lambda_2,\mu}(g_{\lambda_1,\mu}(x)) = 0, \tag{4}$$

$$g'_{\lambda_3,\mu}((g_{\lambda_2,\mu} \circ g_{\lambda_1,\mu})(x)) = 0. \tag{5}$$

It is straightforward to check that the solution of equation (3) is

$$x_0 = \frac{1 - \lambda_1 + \lambda_1 \mu}{2\lambda_1 \mu}.$$

Then, equation (4) reads as

$$g_{\lambda_1,\mu}(x) = \frac{1-\lambda_2+\lambda_2\mu}{2\lambda_2\mu} \tag{6}$$

with solutions

$$x_1^{\pm} = \frac{\lambda_2(1+\lambda_1(\mu-1)) \pm \sqrt{\Delta(\lambda_1,\lambda_2)\lambda_2}}{2\lambda_1\lambda_2\mu},$$

where

$$\Delta(\lambda_1,\lambda_2) = \lambda_2 + \lambda_1(\lambda_1\lambda_2(\mu-1)^2 - 2) > 0.$$

Finally, equation (5) reads as

$$(g_{\lambda_2,\mu} \circ g_{\lambda_1,\mu})(x) = \frac{1-\lambda_3+\lambda_3\mu}{2\lambda_3\mu} \tag{7}$$

with solutions

$$x_2^{\pm} = \frac{\lambda_2\lambda_3(1+\lambda_1(\mu-1)) \pm \sqrt{\lambda_2\lambda_3(\lambda_3\Delta(\lambda_1,\lambda_2) - 2\lambda_1\sqrt{\lambda_3\Delta(\lambda_2,\lambda_3)})}}{2\lambda_1\lambda_2\lambda_3\mu}$$

and

$$x_3^{\pm} = \frac{\lambda_2\lambda_3(1+\lambda_1(\mu-1)) \pm \sqrt{\lambda_2\lambda_3(\lambda_3\Delta(\lambda_1,\lambda_2) + 2\lambda_1\sqrt{\lambda_3\Delta(\lambda_2,\lambda_3)})}}{2\lambda_1\lambda_2\lambda_3\mu},$$

when they exist as real number. It is easy to see that when the seven extrema exist, then

$$x_3^- < x_1^- < x_2^- < x_0 < x_2^+ < x_1^+ < x_3^+.$$

In addition, if $x_3^{\pm}$ are not real, then $x_2^{\pm}$ are also non real. Finally, it is easy to see by equations (6) and (7) that

$$F_{\lambda_1,\lambda_2,\lambda_3,\mu}(x_i^*) = F_{\lambda_1,\lambda_2,\lambda_3,\mu}(x_2^-),\ *\in\{+,-\},\ i\in\{2,3\},$$

and

$$F_{\lambda_1,\lambda_2,\lambda_3,\mu}(x_1^-) = F_{\lambda_1,\lambda_2,\lambda_3,\mu}(x_1^+).$$

We summarize the possible cases as follows. Figure 1 depicts examples of some of these cases.

(C1) $F_{\lambda_1,\lambda_2,\lambda_3,\mu}(x_0) > 0$, $\Delta(\lambda_1,\lambda_2) > 0$ and $\lambda_3\Delta(\lambda_1,\lambda_2) > 2\lambda_1\sqrt{\lambda_3\Delta(\lambda_2,\lambda_3)}$. Then $F_{\lambda_1,\lambda_2,\lambda_3,\mu}$ has 4 maxima, $x_2^{\pm}$ and $x_3^{\pm}$ and 3 minima, $x_1^{\pm}$ and x_0.

(C2) $F_{\lambda_1,\lambda_2,\lambda_3,\mu}(x_0) > 0$, $\Delta(\lambda_1,\lambda_2) > 0$, $\lambda_3\Delta(\lambda_1,\lambda_2) \leq 2\lambda_1\sqrt{\lambda_3\Delta(\lambda_2,\lambda_3)}$ and $\lambda_3\Delta(\lambda_1,\lambda_2) > -2\lambda_1\sqrt{\lambda_3\Delta(\lambda_2,\lambda_3)}$. Then $F_{\lambda_1,\lambda_2,\lambda_3,\mu}$ has 3 maxima, $x_3^{\pm}$ and x_0 and 2 minima, $x_1^{\pm}$.

(C3) $F_{\lambda_1,\lambda_2,\lambda_3,\mu}(x_0) > 0$, $\Delta(\lambda_1,\lambda_2) > 0$ and $\lambda_3\Delta(\lambda_1,\lambda_2) \leq -2\lambda_1\sqrt{\lambda_3\Delta(\lambda_2,\lambda_3)}$. Then $F_{\lambda_1,\lambda_2,\lambda_3,\mu}$ has 2 maxima, $x_1^{\pm}$ and one minimum, x_0.

(C4) $F_{\lambda_1,\lambda_2,\lambda_3,\mu}(x_0) > 0$, $\Delta(\lambda_1,\lambda_2) \leq 0$ and $\lambda_3\Delta(\lambda_1,\lambda_2) > -2\lambda_1\sqrt{\lambda_3\Delta(\lambda_2,\lambda_3)}$. Then $F_{\lambda_1,\lambda_2,\lambda_3,\mu}$ has 2 maxima, $x_3^{\pm}$ and one minimum, x_0.

(C5) $F_{\lambda_1,\lambda_2,\lambda_3,\mu}(x_0) > 0$, $\Delta(\lambda_1,\lambda_2) \leq 0$ and $\lambda_3\Delta(\lambda_1,\lambda_2) \leq -2\lambda_1\sqrt{\lambda_3\Delta(\lambda_2,\lambda_3)}$. Then $F_{\lambda_1,\lambda_2,\lambda_3,\mu}$ has one maximum x_0.

(C6) $F_{\lambda_1,\lambda_2,\lambda_3,\mu}(x_0) \leq 0$, $\Delta(\lambda_1,\lambda_2) > 0$ and $\lambda_3\Delta(\lambda_1,\lambda_2) > 2\lambda_1\sqrt{\lambda_3\Delta(\lambda_2,\lambda_3)}$. Then $F_{\lambda_1,\lambda_2,\lambda_3,\mu}$ has 2 maxima, x_2^- and x_3^- and one minimum x_1^- in $[0,c]$.

(C7) $F_{\lambda_1,\lambda_2,\lambda_3,\mu}(x_0) \leq 0$, $\Delta(\lambda_1,\lambda_2) > 0$ and $\lambda_3\Delta(\lambda_1,\lambda_2) \leq -2\lambda_1\sqrt{\lambda_3\Delta(\lambda_2,\lambda_3)}$. Then $F_{\lambda_1,\lambda_2,\lambda_3,\mu}$ has one maximum, x_1^- in $[0,c]$.

(C8) $F_{\lambda_1,\lambda_2,\lambda_3,\mu}(x_0) \leq 0$, $\Delta(\lambda_1,\lambda_2) \leq 0$ and $\lambda_3\Delta(\lambda_1,\lambda_2) > -2\lambda_1\sqrt{\lambda_3\Delta(\lambda_2,\lambda_3)}$. Then $F_{\lambda_1,\lambda_2,\lambda_3,\mu}$ has one maximum, x_3^- in $[0,c]$.

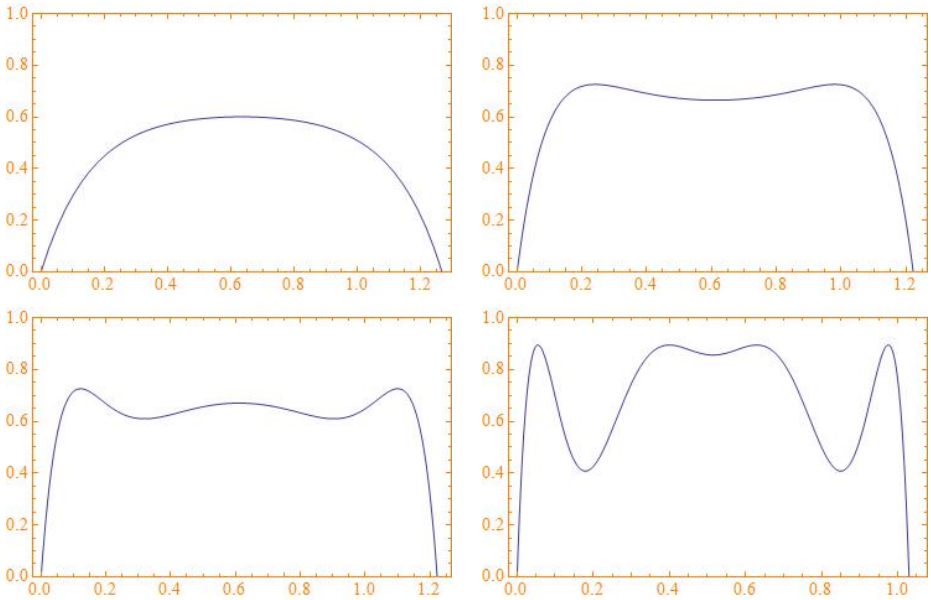

Figure 1: *Different graphs of* $F_{\lambda_1,\lambda_2,\lambda_3,\mu}$.

The above classification is necessary because the dynamics of $F_{\lambda_1,\lambda_2,\lambda_3,\mu}$ depends on its extrema displaying different images. The reader is referred to [15] (see also the summary in [11] and the references therein) to check the following facts.

(F1) The Schwarzian derivative $\mathcal{S}(F_{\lambda_1,\lambda_2,\lambda_3,\mu})$ has the same sign as $g_{\lambda_i,\mu}$, $i = 1, 2, 3$. It is given by

$$\mathcal{S}(g_{\lambda_i,\mu})(x) = \frac{g'''_{\lambda_i,\mu}(x)}{g'_{\lambda_i,\mu}(x)} - \frac{3}{2}\left(\frac{g''_{\lambda_i,\mu}(x)}{g'_{\lambda_i,\mu}(x)}\right)^2.$$

As $g_{\lambda_i,\mu}$ is quadratic, we have that $\mathcal{S}(g_{\lambda_i,\mu})(x) < 0$ for all x whose derivative does not vanish. Then, $\mathcal{S}(F_{\lambda_1,\lambda_2,\lambda_3,\mu}) < 0$.

(F2) As $\mathcal{S}(F_{\lambda_1,\lambda_2,\lambda_3,\mu}) < 0$, the Milnor attractors (see [22]) of any orbit, except perhaps the fixed point 0, must attract the orbit of some extrema. Then, the number of such attractors is bounded by 3 for cases (C1) and (C2), 2 in the cases (C3), (C4) and (C6) and one otherwise. There are many possible trajectories that are not attracted by the Milnor attractors, but they lie in a set of zero Lebesgue measure and therefore, we cannot observe them in numerical simulations.

(F3) If x is a maximum or minimum of $F_{\lambda_1,\lambda_2,\lambda_3,\mu}$, then its Lyapunov exponent is given by

$$Lya(x) = \limsup_{n\to\infty} \frac{1}{n} \log |(F^n_{\lambda_1,\lambda_2,\lambda_3,\mu})'(f(x))|.$$

When the orbit of x is attracted by a periodic orbit it is negative. Then, positive Lyapunov exponents is necessary to have a complicated dynamical behavior.

(F4) The topological entropy of $F_{\lambda_1,\lambda_2,\lambda_3,\mu}$ can be defined (see [1, Chapter 4]) by

$$h(F_{\lambda_1,\lambda_2,\lambda_3,\mu}) = \lim_{n\to\infty} \frac{1}{n} \log c_n(F_{\lambda_1,\lambda_2,\lambda_3,\mu}),$$

where $c_n(F_{\lambda_1,\lambda_2,\lambda_3,\mu})$ denotes the number of pieces of monotonicity of $F^n_{\lambda_1,\lambda_2,\lambda_3,\mu}$. Since $F_{\lambda_1,\lambda_2,\lambda_3,\mu}$ is a polynomial, its extrema are non-flat (i.e. they have a non-null nth derivative for some n). Then, $h(F_{\lambda_1,\lambda_2,\lambda_3,\mu}) > 0$ if and only if $F_{\lambda_1,\lambda_2,\lambda_3,\mu}$ is chaotic in the sense of Li and Yorke (see [21]).

The above definition of topological entropy is not suitable for computing it. So, we use the algorithms to compute it with prescribed accuracy that can be found in [4] for the cases (C5), (C7) and (C8), theone from [9] for the cases (C3), (C4) and (C6) and the one from [10] for the remaining cases.

(F5) Chaos is a topological notion. So, it can happen that $h(F_{\lambda_1,\lambda_2,\lambda_3,\mu}) > 0$ while $Lya(x)$ for all the extrema x of $F_{\lambda_1,\lambda_2,\lambda_3,\mu}$. In this case, we say that chaos is not physically observable.

Taking into account all the above facts, we can compute the topological entropy of $F_{\lambda_1,\lambda_2,\lambda_3,\mu}$. The parameter regions where the topological entropy is positive are capable to exhibit chaos, although it is not always physically observable.

3 The dynamics of $F_{\lambda_1,\lambda_2,\lambda_3,\mu}$

3.1 The case $\lambda_1 = \lambda_2 = \lambda_3 = \lambda$

Here, we consider the case $\lambda_1 = \lambda_2 = \lambda_3 = \lambda$ analyzed in [18]. Let $F_{\lambda,\mu} = F_{\lambda,\lambda,\lambda,\mu} = g^3_{\lambda,\mu}$. It is well-known (see e.g. [1, Chapter 4]) that

$$h(F_{\lambda,\mu}) = 3h(g_{\lambda,\mu}),$$

and therefore $h(F_{\lambda,\mu}) > 0$ if and only if $h(g_{\lambda,\mu}) > 0$. It is enough to compute $h(g_{\lambda,\mu})$, which is shown in Figure 2. This gives us the region where chaotic dynamics is possible. It is also shown the estimations of the Lyapunov exponents. The parameter values with positive topological entropy but negative Lyapunov exponents are those for which chaos is not observed physically. This situation is common along the paper, although for most of the cases we only depict the topological entropy.

Table 1 shows the values of μ and λ_0 for which $h(g_{\lambda,\mu}) > 0$ when $\lambda > \lambda_0$.

μ	λ_0
4	0.85664895
3.9	0.88618857
3.8	0.91783816
3.7	0.95183216
3.6	0.98844104

Table 1. *Values of λ_0 for which $h(g_{\lambda,\mu}) > 0$ when $\lambda > \lambda_0$.*

Note that

$$x_1^{\pm} = \frac{(1 + \lambda(\mu - 1)) \pm \sqrt{\Delta(\lambda)}}{2\lambda\mu},$$

where

$$\Delta(\lambda) = \lambda^2(\mu - 1)^2 - 1,$$

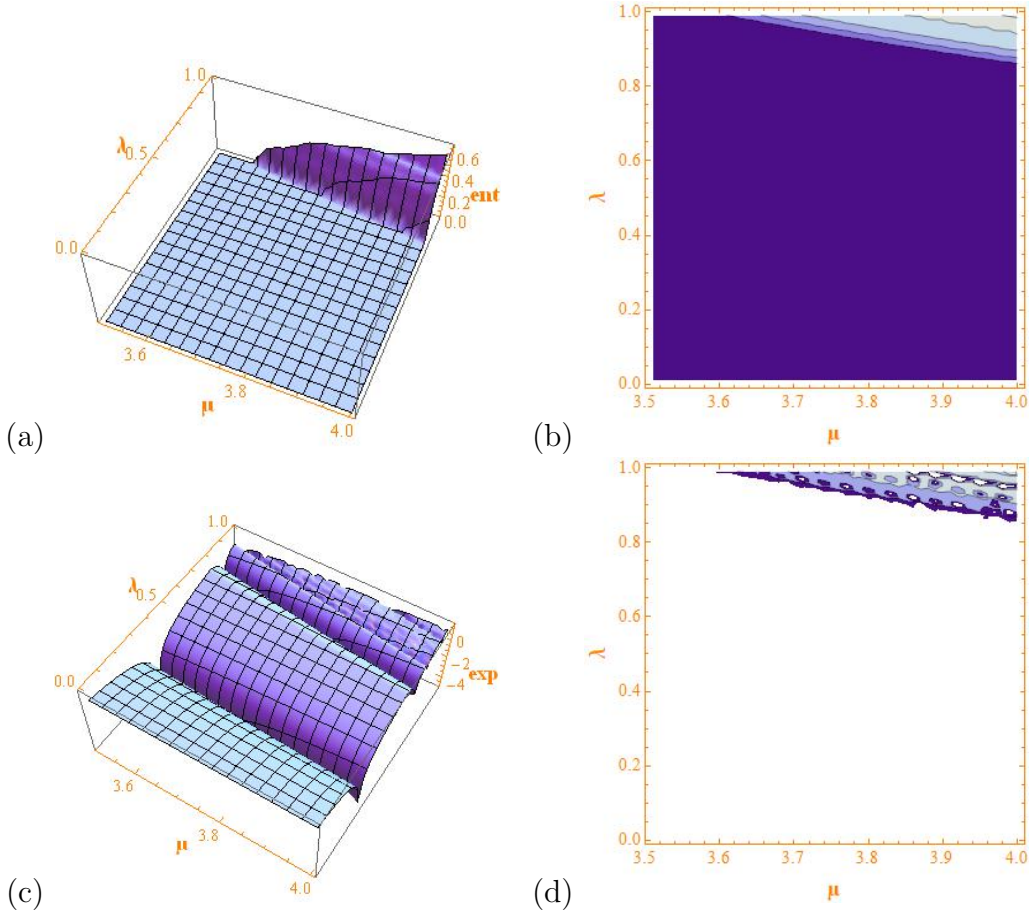

Figure 2: *(a)-(b) Graph and level curves of the topological entropy of $g_{\lambda,\mu}$ with accuracy 10^{-6}. (c)-(d) Graph and level curves of the estimation of the maximum Lyapunov exponent of $g_{\lambda,\mu}$. The step size for λ and μ is 10^{-2}.*

and

$$x_2^{\pm} = \frac{(1+\lambda(\mu-1)) \pm \sqrt{\Delta(\lambda) - 2\sqrt{\Delta(\lambda)}}}{2\lambda\mu}$$

and

$$x_3^{\pm} = \frac{(1+\lambda(\mu-1)) \pm \sqrt{\Delta(\lambda) + 2\sqrt{\Delta(\lambda)}}}{2\lambda\mu}.$$

It is easy to see that $\Delta(\lambda) > 0$ and $\Delta(\lambda) + 2\sqrt{\Delta(\lambda)} > 0$ when

$$\mu > \frac{1+\lambda}{\lambda}$$

while $\Delta(\lambda) - 2\sqrt{\Delta(\lambda)} > 0$ when

$$\mu > \frac{\sqrt{5}+\lambda}{\lambda}.$$

So, it is possible to have three different bifurcation diagrams when $x_i^{\pm}$, $i \in \{1,2,3\}$ exist. For instance, Figure 3 shows and example of this fact.

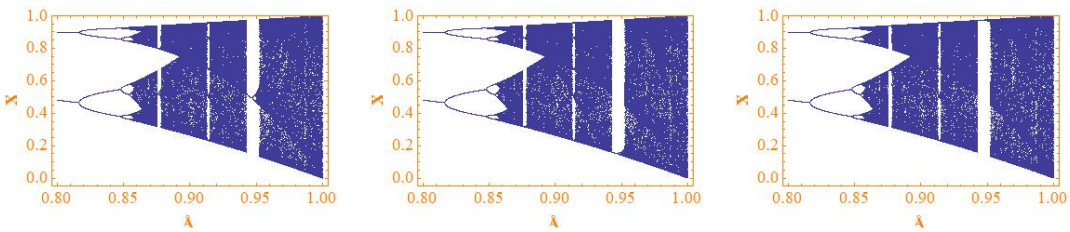

Figure 3: *Three different bifurcation diagrams when $\mu = 4$ (note the differences around 0.879 and, more evident, 0.95). The parameter λ ranges $[0.8, 1]$ with step size 10^{-4}. We compute 100000 points of each orbit and plot the last 100.*

3.2 The case $\lambda_1 = \lambda_2 = \lambda$

Next, we will assume that $\lambda_1 = \lambda_2 = \lambda$ and let $F_{\lambda,\lambda_3,\mu} = F_{\lambda_1,\lambda_2,\lambda_3,\mu}$. Now, we fix the parameter μ and check how the dynamics of $F_{\lambda,\lambda_3,\mu}$ changes when λ and λ_3 vary. We fix $\mu = 4$ and show in Figure 4 the computation of the topological entropy and the estimation of the Lyapunov exponents.

Figure 4 gives the region where the map $F_{\lambda,\lambda_3,\mu}$ can be chaotic, provided by positive topological entropy. The colored region of Lyapunov exponents shows

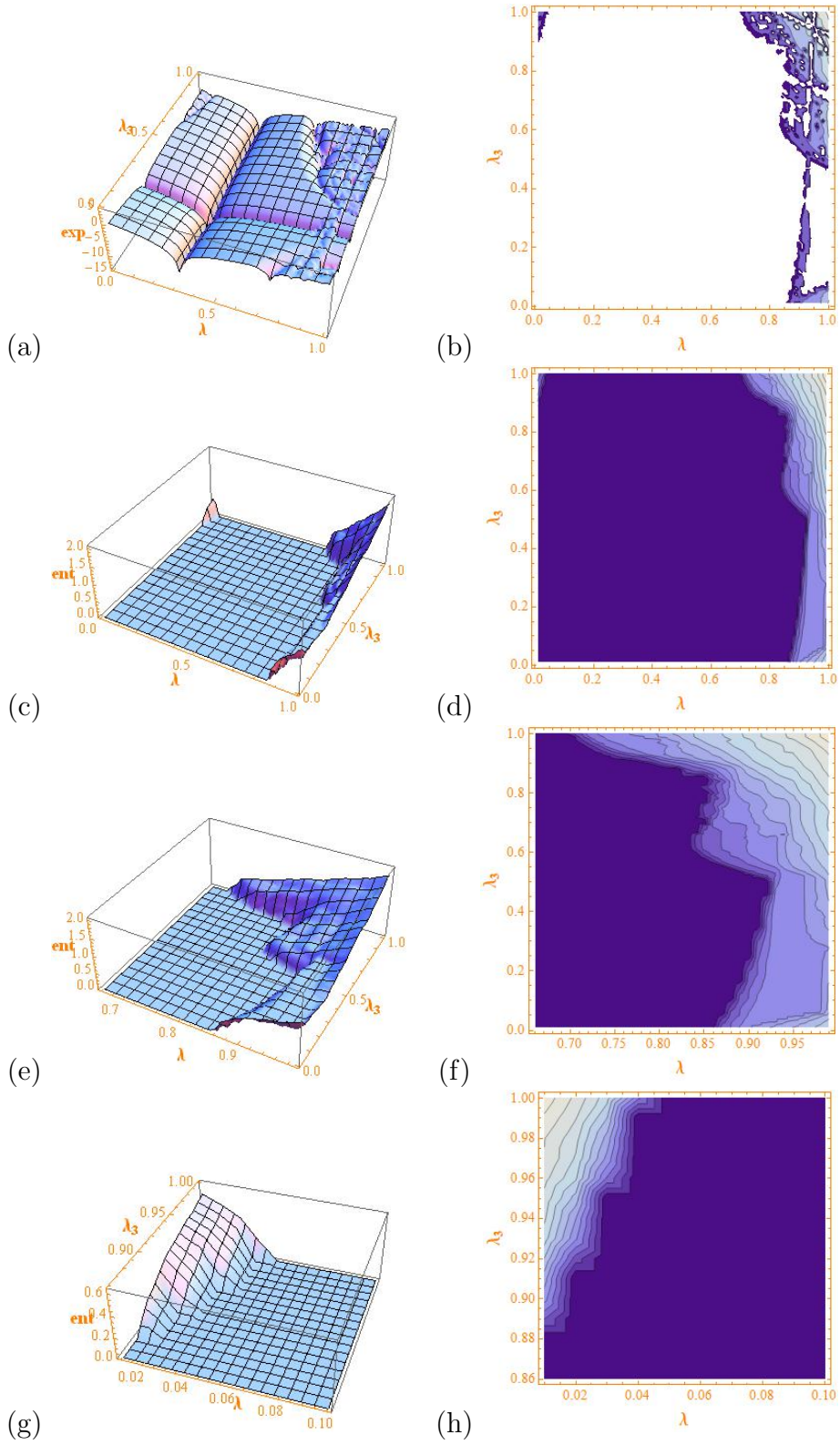

Figure 4: *(a)-(b) Graph and level curves of the estimation of the maximum Lyapunov exponent of* $F_{\lambda,\lambda_3,4}$*. (c)-(d) Graph and level curves of the topological entropy of* $F_{\lambda,\lambda_3,4}$ *with accuracy* 10^{-3}*. (e)-(f) and (g)-(h) depict a zoom of the region where the topological entropy can be positive. The step size for* λ *and* λ_3 *is* 10^{-2}*.*

when this chaos can be physically observable. We will not show more figures with estimations of Lyapunov exponents.

Note that for $\mu = 4$, the map $g_{\lambda,4}$ has positive topological entropy when $\lambda_0 > 0.85664895$. The zoomed region of Figure 4 (g)-(h) shows that $F_{\lambda,\lambda_3,4}$ may have positive topological entropy for these parameter values. But note that $\lambda_3 > \lambda_0$, and therefore $g_{\lambda_3,4}$ is also chaotic. It is remarkable that we can obtain positive values of entropy with parameter λ_3 close to zero, and hence $g_{\lambda_3,\mu}$ close to the identity.

The zoomed region of Figure 4 (e)-(f) shows the existence of parameter values for which the map $F_{\lambda,\lambda_3,4}$ has positive entropy when λ and λ_3 are both smaller than λ_0. In particular, when λ is close enough to 0.84 and λ_3 to 0.62. This is an example of "simple + simple = complex" paradox. This is not only for $\mu = 4$. Figure 5 shows this zoomed region where Parrondo's paradox is possible for several values of μ. Table 2 shows the values of μ, λ and λ_3 for which $h(F_{\lambda,\lambda_3,\mu}) > 0$. The topological entropy remains positive in a suitable neighborhood of these values.

μ	λ	λ_3
3.9	0.87	0.65
3.8	0.90	0.67
3.7	0.94	0.72
3.6	0.97	0.74

Table 2. *Values of μ, λ and λ_3 for which $h(F_{\lambda,\lambda_3,\mu}) > 0$.*

Finally, it is remarkable that non chaotic parameter values μ can be destabilized. For instance, for $\mu = 3.5$ we depict in Figure 6 the computation of the topological entropy of $F_{\lambda,\lambda_3,3.5}$. Clearly $h(g_{\lambda_1,3.5}) = h(g_{\lambda_3,3.5}) = 0$, while $h(F_{\lambda_1,\lambda_2,\lambda_3,3.5}) > 0$. This is another example of the Parrondo's paradoxical phenomenon.

3.3 The general case

Now, we assume that the parameters λ_1, λ_2 and λ_3 need not be the same. Note that by [17], we have that

$$h(F_{\lambda_1,\lambda_2,\lambda_3,\mu}) = h(F_{\lambda_2,\lambda_3,\lambda_1,\mu}) = h(F_{\lambda_3,\lambda_1,\lambda_2,\mu}).$$

Hence, all the parameters λ_1, λ_2 and λ_3 play the same role. This allows us to fix $\lambda_3 = \lambda$ and vary the parameters λ_1 and λ_2 within $(0, 1)$. In the previous section we check that when μ decreases, so it does the region where the dynamic is complex. So, we will focuss on the variation of λ. For that, we consider a fixed value of $\mu = 3.9$. Figure 7 shows the computation of the topological entropy for some values of λ.

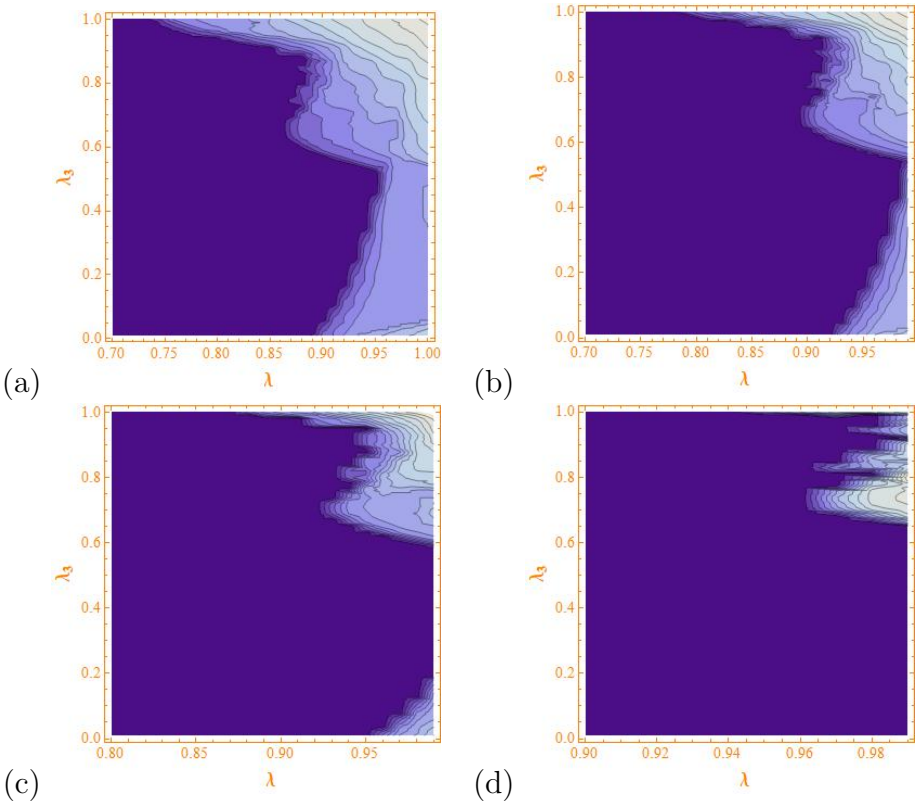

Figure 5: *Level curves of the topological entropy of* $F_{\lambda,\lambda_3,\mu}$ *when* $\mu = 3.9$*(a),* 3.8*(b),* 3.7*(c) and* 3.6*(d). The accuracy is* 10^{-3} *and the step size for* λ *and* λ_3 *is* 10^{-2}*. Note the different size of the intervals for* λ*.*

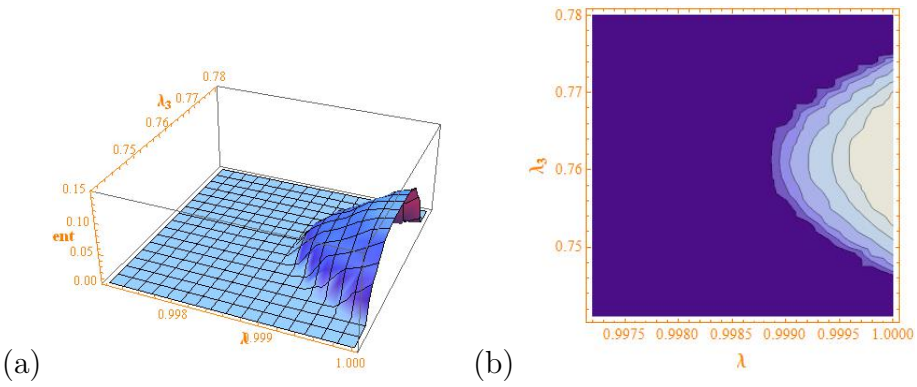

Figure 6: *Graph and level curves of the estimation of the topological entropy of* $F_{\lambda,\lambda_3,3.5}$ *for* $\lambda \in [0.9975, 1]$ *and* $\lambda_3 \in [0.74, 0.78]$*. The accuracy is* 10^{-3} *and the step size for* λ *and* λ_3 *is* 10^{-3}*.*

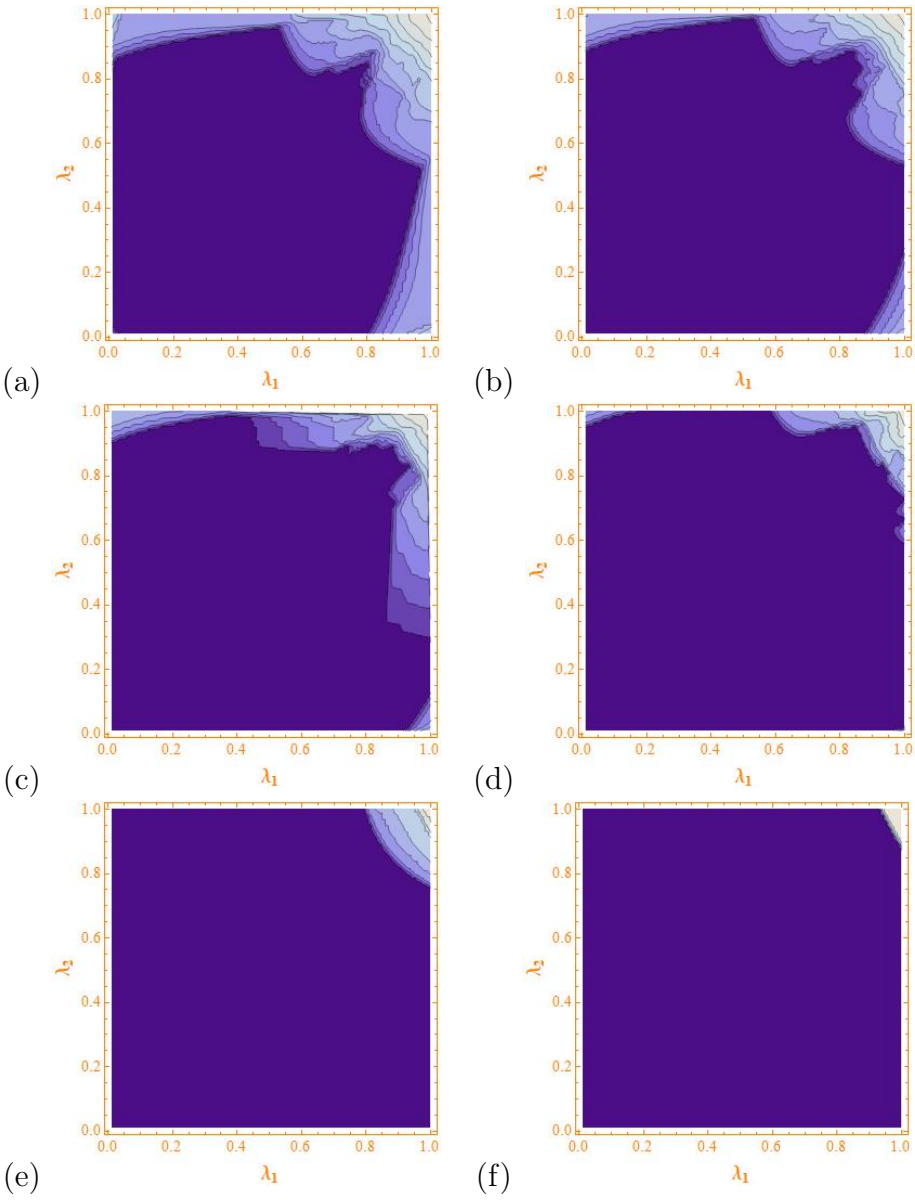

Figure 7: *Level curves of the topological entropy of* $F_{\lambda,\lambda_3,\mu}$ *when* $mu = 3.9$ *and* $\lambda_3 = 0.95$*(a),* 0.9*(b),* 0.87*(c),* 0.8*(d),* 0.65*(e) and* 0.5*(f). The accuracy is* 10^{-3} *and the step size for* λ_1 *and* λ_2 *is* 10^{-2}.

Our computations suggest that when $\lambda = \lambda_3$ decreases, so it does the area of the parameter region where the topological entropy is positive. Note that when $\lambda < \lambda_0 = 0.88618857$ the map $g_{\lambda,3.9}$ has zero topological entropy and Figure 7 (c), (d) and (e) shows that we can obtain positive topological entropy for all the values $\lambda_i < \lambda_0$, $i = 1, 2, 3$. This is again a new example of the Parrondo's paradox "simple + simple =complex". Note that the values of $\lambda = \lambda_3$ 0.87 and 0.65 come from Table 2. Figure 8 shows bifurcation diagrams for these values.

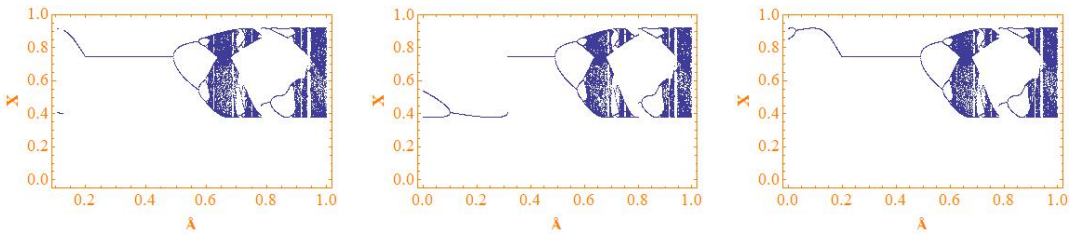

Figure 8: *Bifurcation diagrams when* $\mu = 3.9$. *The parameter* λ_1 *ranges* $[0, 1]$ *with step size* 10^{-3}, $\lambda_2 = 0.87$ *and* $\lambda_3 = 0.88$. *We compute 100000 points of each orbit with initial condition belonging to the set of extrema and plot the last 100. Note the chaotic behavior can be seen around* $\lambda_1 = 0.65$.

Finally, note that the graphs of Figure 7 are not symmetric with respect to the diagonal of the square. So, there can exist values of λ_i, $i = 1, 2, 3$ such that $F_{\lambda_1,\lambda_2,\lambda_3,\mu}$ is chaotic while $F_{\lambda_2,\lambda_1,\lambda_3,\mu}$ is not. It suffices to take $\lambda_1 = 0.85$, $\lambda_2 = 0.78$ and $\lambda_3 = 0.87$, which gives us $h(F_{\lambda_1,\lambda_2,\lambda_3,3.9}) = 0.12022146651591863$ while $h(F_{\lambda_2,\lambda_1,\lambda_3,3.9}) = 0$.

4 Conclusion

Although the map $g_{\lambda,\mu}$ is useful in controlling the chaotic dynamics of the logistic family f_μ, it must be carefully handled if we want to apply it with different values of λ. Here, the "simple + simple = complex" Parrondo's paradox can produce undesirable dynamics. In general, if λ cannot be fixed, we should take these values in an open open interval with suitable length, as the mentioned paradox is only possible for different enough λ's. We want to mention that this study can be adapted for other chaotic maps different from the logistic family.

Declarations

J.S. Cánovas was supported by the project MTM 2017-84079-P Agencia Estatal de Investigación (AEI) y Fondo Europeo de Desarrollo Regional (FEDER).

The author declares that he does not have any conflict of interest, no data has been used except the one generated for making the computations, and the software Mathematica has been used.

References

[1] L. Alsedá, J. Llibre and M. Misiurewicz, *Combinatorial dynamics and entropy in dimension one,* World Scientific Publishing, 1993.

[2] G. Blé, V. Castellanos and M. Falconi, *On the coexisting dynamics in the alternate iteration of two logistic maps*, Dyn. Syst. **26** (2011), 189-197.

[3] G. Blé, F. E. Castillo-Santos, D. González and R. Valdez, *On a quartic polynomials family of two parameters*, Dyn. Syst. DOI: 10.1080/14689367.2020.1849031 (2020).

[4] L. Block, J. Keesling, S. H. Li, and K. Peterson, *An improved algorithm for computing topological entropy,* J. Stat. Phys., **55** (1989), 929-939.

[5] J. S. Cánovas, *Periodic sequences of simple maps can support chaos*, Physica A: Statistical Mechanics and its Applications **466** (2017), 153-159.

[6] J. S. Cánovas, *On the Periodic Ricker Equation*, International Conference in Nonlinear Analysis and Boundary Value Problems, 121-130 (2018), Springer, Cham.

[7] J. S. Cánovas, A. Linero and D. Peralta-Salas, *Dynamic Parrondo's paradox*, Physica D: Nonlinear Phenomena **218** (2006), 177-184.

[8] J. S. Cánovas and M. Muñoz, *Revisiting Parrondo's paradox for the logistic family*, Fluctuation and Noise Letters **12** (2013), 1350015.

[9] J. S. Cánovas and M. Muñoz–Guillermo,*Computing topological entropy for periodic sequences of unimodal maps,* Communications in Nonlinear Science and Numerical Simulation. 19 (2014) 3119–3127.

[10] J. S. Cánovas and M. Muñoz–Guillermo,*Computing the topological entropy of continuous maps with at most three different kneading sequences with applications to Parrondo's paradox,* Chaos, Solitons & Fractals **83** (2016), 1–17.

[11] J. S. Cánovas and M. Muñoz–Guillermo,*On the dynamics of Kopel's Cournot duopoly model,* Applied Mathematics and Computation **330** (2018), 292-306.

[12] J. S. Cánovas and M. Muñoz, *On the dynamics of the q-deformed logistic map*, Physics Letters A **383** (2019), 1742-1754.

[13] K. H. Cheong, T. Wen and J. W. Lai, *Relieving Cost of Epidemic by Parrondo's Paradox: A COVID-19 Case Study*, Advanced Science (2020), 2002324

[14] A. Cima, A. Gasull, V. Mañosa, *Parrondo's dynamic paradox for the stability of non-hyperbolic fixed points*, arXiv:1701.05816.

[15] W. de Melo and S. van Strien, *One dimensional dynamics,* (1993) Springer Verlag.

[16] A. Gasull, L. Hernández-Corbato, F. R. Ruiz del Portal, *Parrondo's paradox for homeomorphisms*, arXiv:2010.12893.

[17] S. Kolyada and L'. Snoha, *Topological entropy of nonautononous dynamical systems,* Random and Comp. Dynamics **4** (1996), 205-233.

[18] S. Kumari and R. Chugh, *A novel four-step feedback procedure for rapid control of chaotic behavior of the logistic map and unstable traffic on the road,* Chaos **30** (2020), 123115.

[19] J. W. Lai and K. H. Cheong, *Parrondo's paradox from classical to quantum: A review*, Nonlinear Dyn. **100** (2020), 849-861.

[20] J. W. Lai and K. H. Cheong, *Social dynamics and Parrondo's paradox: a narrative review*, Nonlinear Dyn. **101** (2020), 1-20.

[21] T.Y. Li and J. A. Yorke, *Period three implies chaos,* Amer. Math. Monthly **82** (1975) 985-992.

[22] J. Milnor, *On the concept of attractor,* Comm. Math. Phys. **99** (1985) 177-195.

[23] S. A. Mendoza and E. Peacock-López, *Switching induced oscillations in discrete one-dimensional systems,* Chaos, Solitons & Fractals, **115** (2018), 35-44.

[24] W. Phuengrattana and S. Suantai, *On the rate of convergence of Mann, Ishikawa, Noor and SP-iterations for continuous functions on an arbitrary interval,* Journal of Computational and Applied Mathematics **235** (2011), 3006-3014.

[25] E. Peacock-López, *Seasonality as a Parrondian game,* Physics Letters A **375** (2011), 3124-3129.

[26] E. Silva and E. Peacock-López, *Seasonality and the logisitic map,* Chaos, Solitons & Fractals **95** (2017), 152-156.

Figures

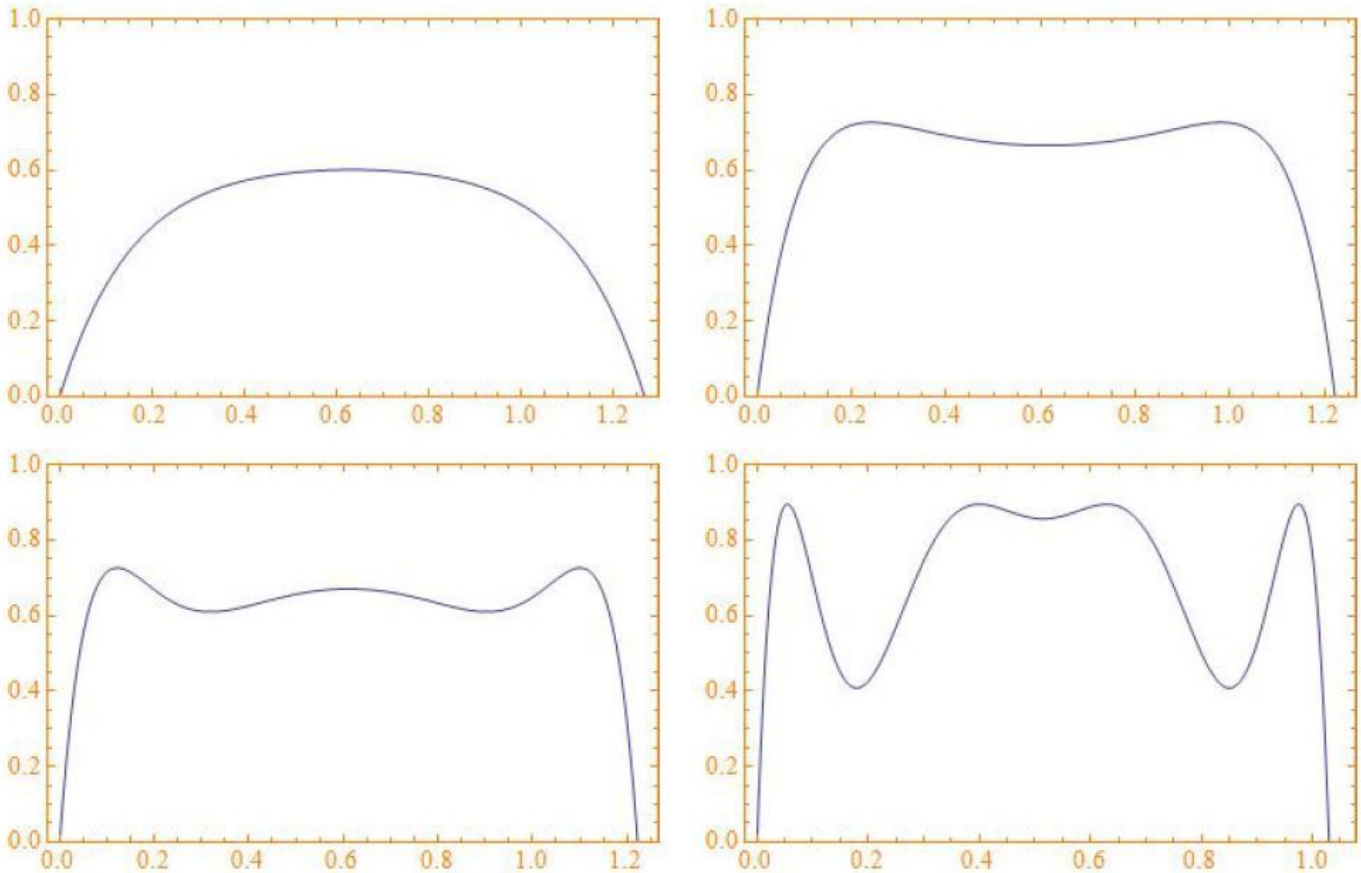

Figure 1

Different graphs of Fλ1;λ2;λ3;μ.

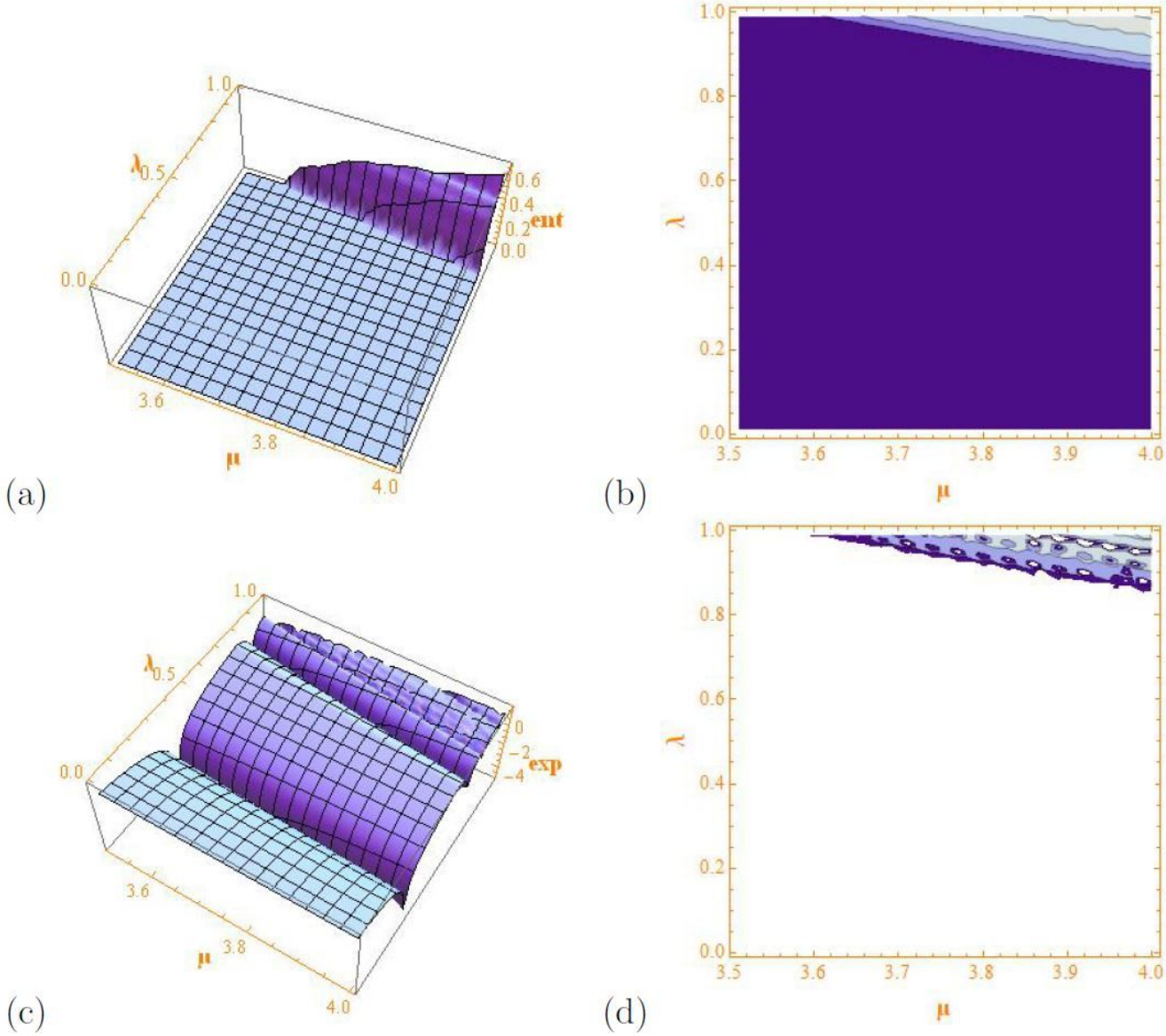

Figure 2

(a)-(b) Graph and level curves of the topological entropy of gλ;μ with accu- racy 10-6. (c)-(d) Graph and level curves of the estimation of the maximum Lyapunov exponent of gλ;μ. The step size for λ and μ is 10-2.

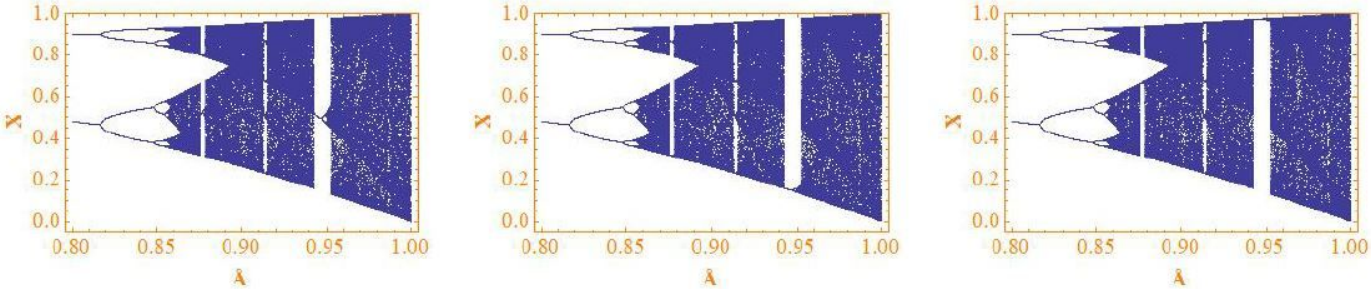

Figure 3

Three different bifurcation diagrams when μ = 4 (note the differences around 0:879 and, more evident, 0:95). The parameter λ ranges [0:8; 1] with step size 10-4. We compute 100000 points of each orbit and plot the last 100.

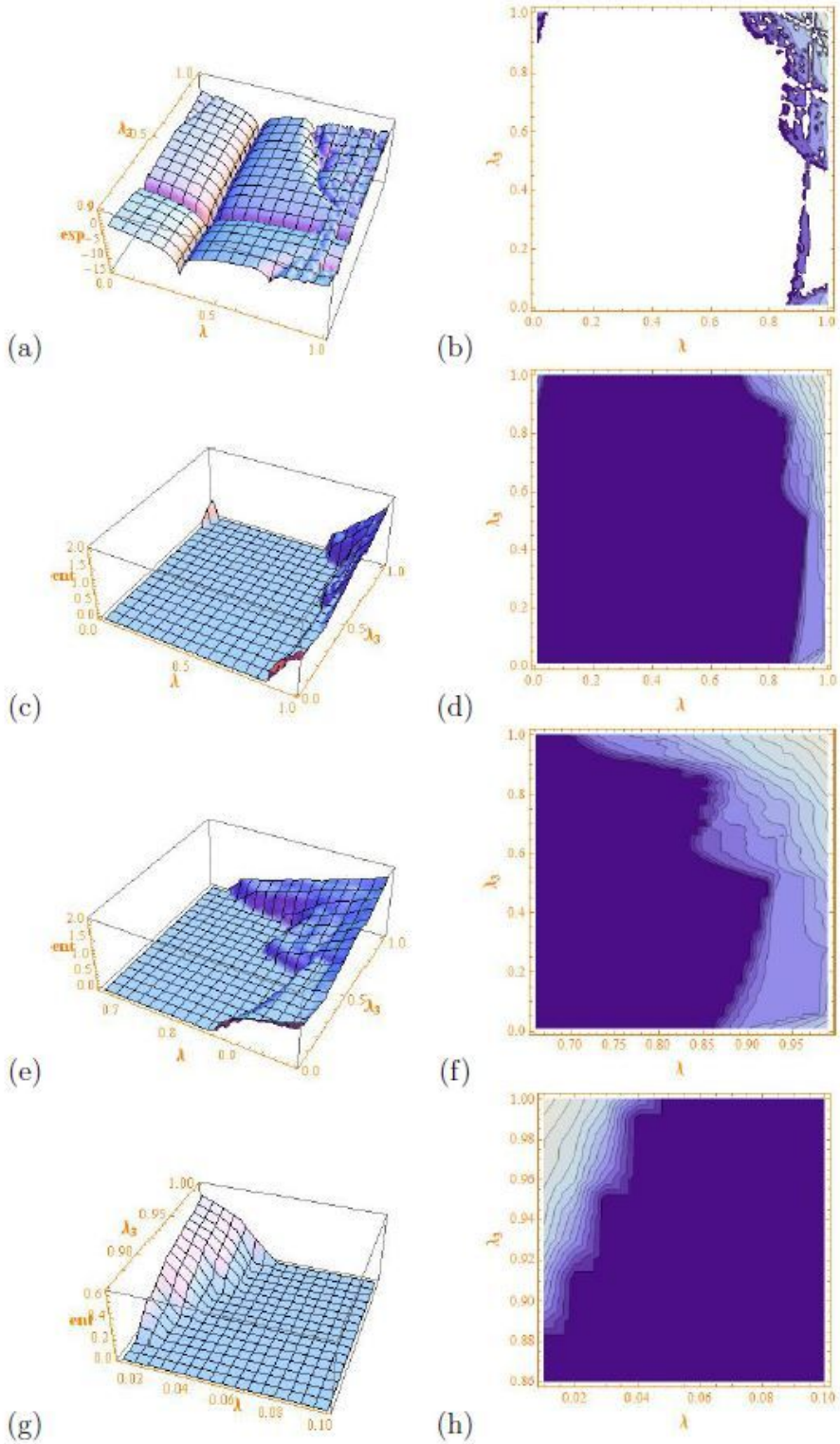

Figure 4

(a)-(b) Graph and level curves of the estimation of the maximum Lyapunov exponent of Fλ;λ3;4. (c)-(d) Graph and level curves of the topological entropy of Fλ;λ3;4 with accuracy 10-3. (e)-(f) and (g)-(h) depict

a zoom of the region where the topological entropy can be positive. The step size for λ and λ3 is 10-2.

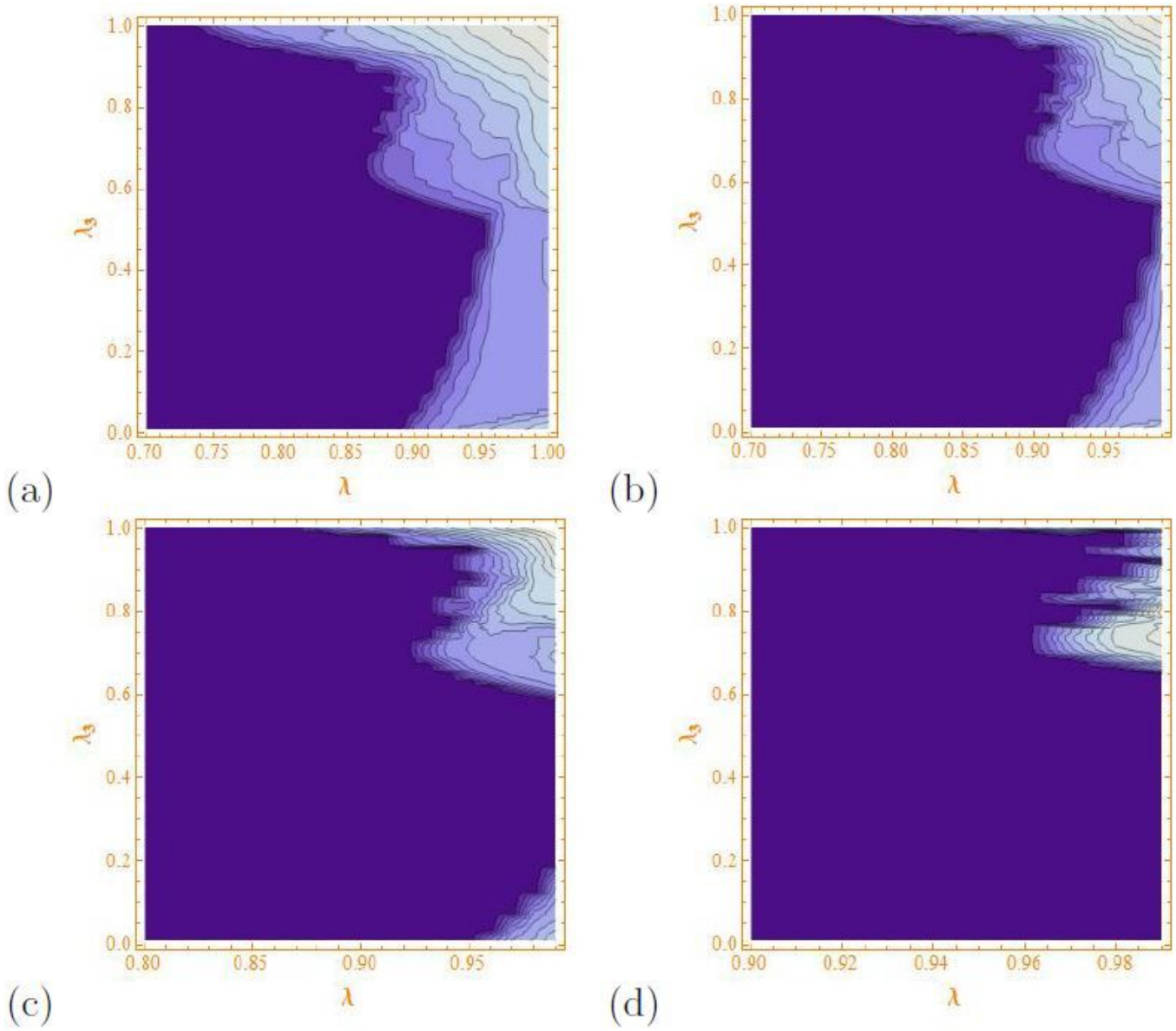

Figure 5

Level curves of the topological entropy of Fλ;λ3;μ when μ = 3:9(a), 3:8(b), 3:7(c) and 3:6(d). The accuracy is 10-3 and the step size for λ and λ3 is 10-2. Note the different size of the intervals for λ.

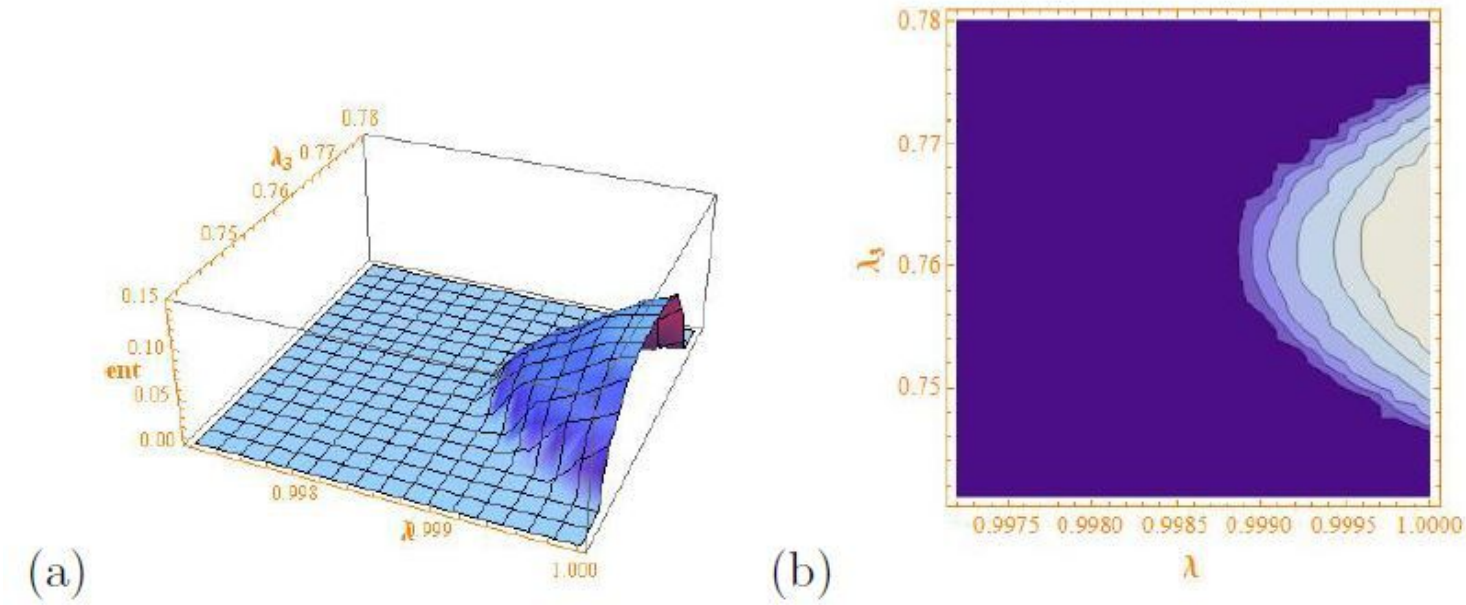

Figure 6

Graph and level curves of the estimation of the topological entropy of Fλ;λ3;3:5 for λ 2 [0:9975; 1] and λ3 2 [0:74; 0:78]. The accuracy is 10-3 and the step size for λ and λ3 is 10-3.

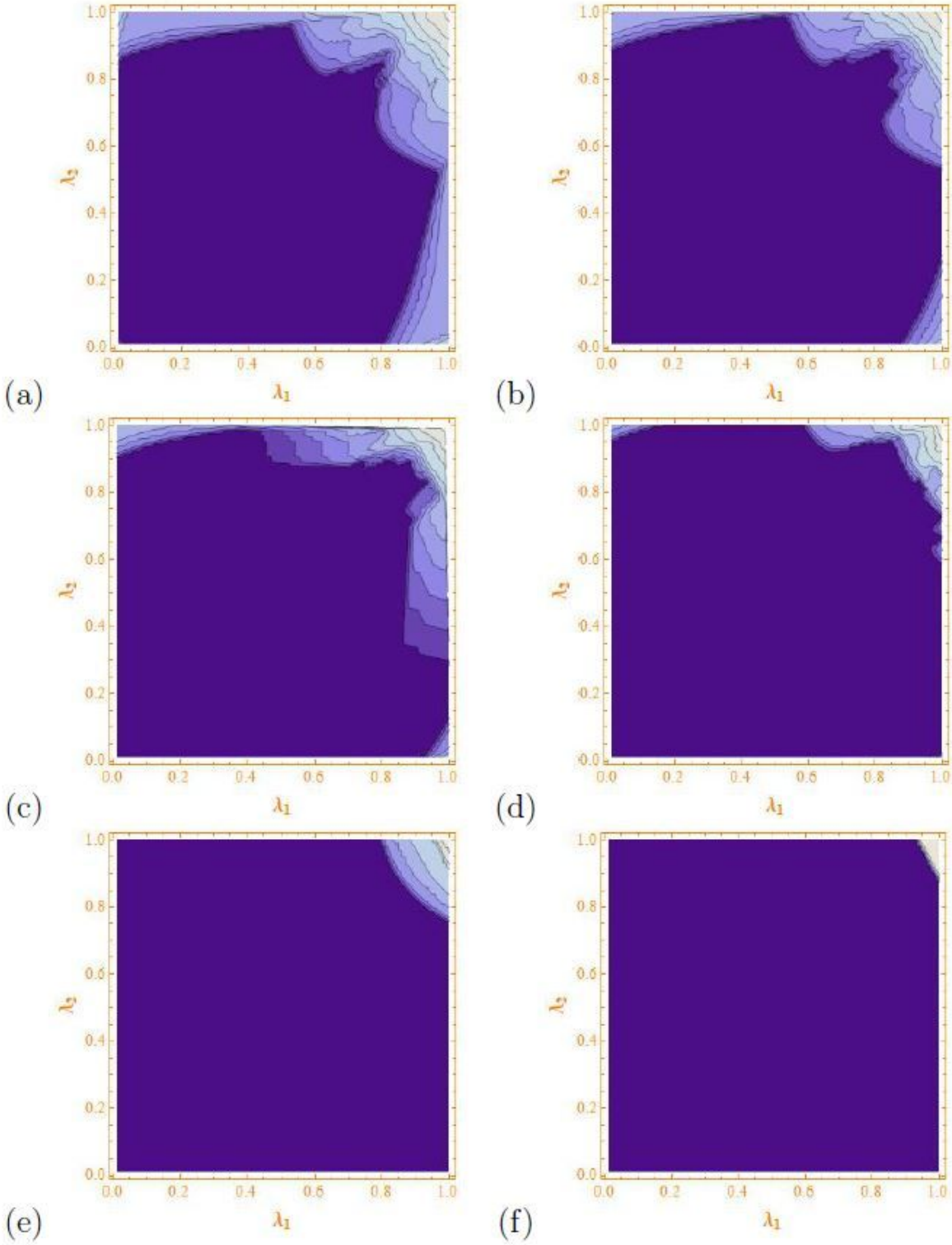

Figure 7

Level curves of the topological entropy of Fλ;λ3;μ when mu = 3:9 and λ3 = 0:95(a), 0:9(b), 0:87(c), 0:8(d), 0:65(e) and 0:5(f). The accuracy is 10-3 and the step size for λ1 and λ2 is 10-2.

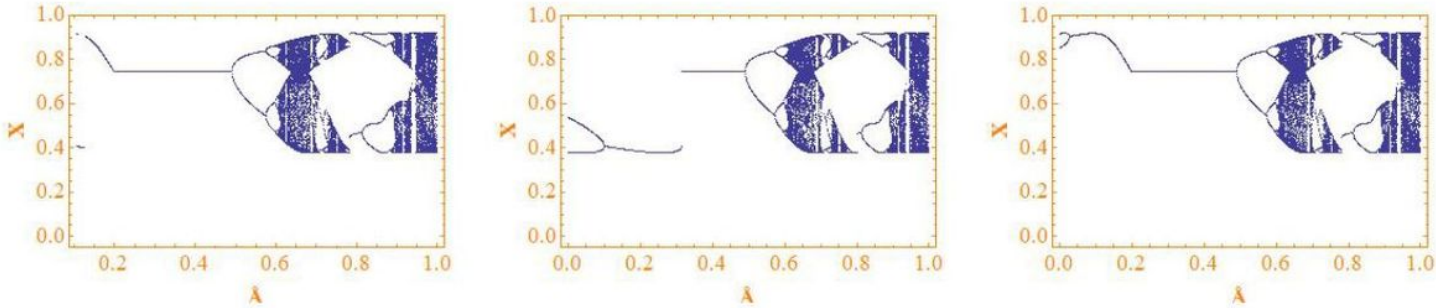

Figure 8

Bifurcation diagrams when μ = 3:9. The parameter λ1 ranges [0; 1] with step size 10-3, λ2 = 0:87 and λ3 = 0:88. We compute 100000 points of each orbit with initial condition belonging to the set of extrema and plot the last 100. Note the chaotic behavior can be seen around λ1 = 0:65.